JOURNAL OF MATERIALS SCIENCE 33 (1998) 2595–2599

Lindeman's melting law and solidus curve under pressure of Al–Si and Al–Ge solid solutions

HIROKO-MATSUO KAGAYA, KAZUMOTO IMAZAWA, MAYUMI SATO, TOSHINOBU SOMA
Department of Computer Science and Engineering, Mining College, Akita University, Akita 010, Japan

Using the pressure dependence of the mean-square displacement, the compression effect on the melting temperature of matrix Al is studied by Lindeman's melting law. The melting curve obtained increases as a function of the pressure and is in good agreement with the observed tendency for Al. The contribution of the transverse-like acoustic modes to the mean-square displacement is important for Al and becomes more predominant under pressure. Then, considering the contributions from the band and local mode frequencies, the temperature- and pressure-dependent mean-square displacement is quantitatively calculated for Al–Si and Al–Ge solid solutions. The concentration dependence of the Debye temperature at high and low temperatures is estimated, and the pressure effect on the solidus curves is presented by applying Lindeman's melting law to the Al–Si and Al–Ge alloy systems. © *1998 Chapman & Hall*

1. Introduction

The mean-square displacement of thermal vibration is important for anharmonic and melting properties. As the temperature is raised, the root-mean-square displacement becomes large, and the contributions to the free energy from the anharmonic term produce the thermal expansion. The increase in the root-mean-square displacement at higher temperatures causes fusion of the solid lattice according to Lindeman's [1] melting law. The pressure effect on the melting point was experimentally reported (see, for example, [2]), and the qualitative tendency is not unique for all solids. The melting point of covalent crystals decreases under increasing pressure, but that of metallic materials increases. Previously, some experimental studies [3–5] about the mean-square displacements of Al from the X-ray Debye–Waller factor have been reported, and the effect of pressure on the melting temperature of Al in the low-pressure regions has also been obtained experimentally [6, 7].

Under pressure, by rapid quenching from the liquid state, an increase in solubility limit of Si and Ge in Al has been observed [8–10]. Previously, using the pseudopotential formalism and the virtual-crystal approximation, we [11] have obtained good agreement of the equilibrium volume, equation of state and phase boundary of Al–Si and Al–Ge alloy systems with experimental data and, considering the lattice dynamical contributions to the free energy, presented the temperature- and concentration-dependent elastic constants for $Al_{1-x}Si_x$ and $Al_{1-x}Ge_x$ alloy systems [12]. Then, we [13] have proposed a simplified treatment where the lattice vibrations of Al, Si or Ge atoms in the Al–Si and Al–Ge solid solutions are replaced by that of pure Al, face-centred cubic (f.c.c.) Si or f.c.c. Ge crystal at the lattice constant and electron density of the alloy. In the present work, first, we calculate the temperature dependence of the mean-square displacement for matrix Al. Then, using the pressure-dependent mean-square displacement, we study the effect of compression on the melting temperature of Al with the f.c.c. phase according to Lindeman's [1] criterion for melting. Secondly, considering the contributions from the band and local mode frequencies [13], we calculate the concentration- and pressure-dependent mean-square displacement for Al–Si and Al–Ge solid solutions. Finally, by applying Lindeman's melting law to the Al–Si and Al–Ge alloy systems, we study the pressure effect on the solidus curves of these systems.

2. Lindeman's criterion and melting of matrix Al

The mean-square displacement, $\langle u^2 \rangle$, is temperature dependent and can be expressed in terms of the ith phonon mode frequency, $\nu_i(\boldsymbol{q})$ with wavevector $\boldsymbol{q}$, for a monatomic cubic crystal as

$$\langle u^2 \rangle = \frac{h}{NM} \sum_{i,q} \frac{1}{\nu_i(\boldsymbol{q})} \left(\frac{1}{\exp[h\nu_i(\boldsymbol{q})/kT] - 1} + \frac{1}{2} \right) \tag{1}$$

where the summation is over all the N $\boldsymbol{q}$ points in the Brillouin zone and all three i branches of the phonon dispersion curves $\nu_i(\boldsymbol{q})$. In order to calculate $\nu_i(\boldsymbol{q})$, we adopt our previous treatment [11–13] based on the microscopic electronic theory. In numerical calculations, we use the following sampling method.

Considering the symmetry of the irreducible one-forty eighth portion of the Brillouin zone, it is sufficient to determine the phonon frequencies in the range $\boldsymbol{q} = 2\pi(q_x, q_y, q_z)/16a$, where q_x, q_y and q_z are positive integers and satisfy the inequalities $0 \leqslant q_x \leqslant q_y \leqslant q_z \leqslant 16$ and $q_x + q_y + q_z \leqslant 24$, and a is the lattice constant. Each point is weighted according to the number of points equivalent to it by symmetry, especially on the surface, edges and corners of the Brillouin zone. A divergence occurs for the $q \approx 0$ acoustic mode phonon in the sum over the wavevector mesh of Equation 1. Therefore, the contribution to the mean-square displacement owing to $q \approx 0$ mode frequencies is calculated by converting the summation to an integral and assuming a Debye distribution.

We show the temperature dependence of $\langle u^2 \rangle$ for matrix Al obtained using Equation 1 in Fig. 1, where points are observed data [3–5], and T_m is the melting temperature at atmospheric pressure. In this figure and what follows, the results with Vashishta–Singwi screening function [11] are given, and our obtained mean-square displacement, $\langle u^2 \rangle$, has a calculated accuracy $|\langle u^2 \rangle| \leqslant 10^{-20}\,\text{cm}^2$ at $T = 0$ and $|\langle u^2 \rangle| \leqslant 2 \times 10^{-19}\,\text{cm}^2$ at $T = T_m$ due to other screening functions [11]. In Fig. 1, the separate contributions, $\langle u^2 \rangle_{TA}$ and $\langle u^2 \rangle_{LA}$, to the total mean-square displacement, $\langle u^2 \rangle$, from transverse-like and longitudinal-like acoustic modes are also given, and we see that the contribution of the transverse-like acoustic modes to the mean-square displacement is predominant for Al. In Debye's model, the mean-square displacement, $\langle u^2 \rangle$, is related to the Debye temperature, Θ_D, given (see, for example, [14]) by

$$\langle u^2 \rangle = \frac{9\hbar^2 T}{Mk\Theta_D^2} \quad \text{for} \quad T > \Theta_D \tag{2}$$

or

$$\langle u^2 \rangle = \frac{9\hbar^2}{4Mk\Theta_D} \quad \text{for} \quad T < \Theta_D \tag{3}$$

Lindeman [1] proposed that the melting process occurs when the root-mean-square displacement, $\langle u^2 \rangle^{1/2}$, of the lattice vibration reaches a critical fraction of the nearest-neighbour distance. He assumed that this critical fraction was the same for all crystalline solids, but it was later shown (see, for example, [15, 16]) that in various cubic metals and alkali halides this fraction was actually not constant. We define Lindeman's criterion for melting, x_m, as the ratio of two times the root-mean-square displacement, $\langle u^2 \rangle^{1/2}$, at the melting temperature, T_m, to the nearest-neighbour distance, R_1 ($= 2^{1/2}a/2$), given by

$$x_m = \frac{2\langle u^2 \rangle^{1/2}}{R_1} \tag{4}$$

The numerical data of the critical fraction, x_m, for melting obtained is 0.2216 ± 0.0005 for matrix Al. We calculate the dependence of the phonon frequencies, $\nu_i(\boldsymbol{q})$ [13], on the pressure, P. The conversion to the compressed volume is performed using the pressure–volume relation [11]. Using Equation 1, we show the temperature dependence of the mean-square displacement, $\langle u^2 \rangle$, under pressure for matrix Al in Fig. 2. Then, we show the relative contributions $\langle u^2 \rangle_{TA}/\langle u^2 \rangle$ and $\langle u^2 \rangle_{LA}/\langle u^2 \rangle$, to the total mean-square displacement from the transverse-like and longitudinal-like acoustic modes at the melting temperature under atmospheric pressure against the pressure in Fig. 3. From this figure, we see that the contribution of the transverse-like acoustic modes becomes more predominant as the crystal is compressed.

Considering the pressure dependence of the mean-square displacement, $\langle u^2 \rangle$, and the nearest-neighbour distance, R_1, at a constant criterion for melting, x_m, we can estimate the pressure effect on the melting temperature by satisfying the following relations

$$x_m = \frac{2\langle u^2 \rangle^{1/2}_{T_m(P)}}{R_1(P)} \tag{5}$$

and

$$R_1(P) = \left(\frac{\Omega(P)}{\Omega_0}\right)^{1/3} R_1(\Omega_0) \tag{6}$$

where Ω_0 and $\Omega(P)$ are the crystal volume under atmospheric pressure and under pressure, P, respectively. We show the result obtained for the pressure dependence of the melting temperature in Fig. 4, where the maximum deviation of the melting temperature obtained is about $\pm$ 5 K and the full and open circles are the observed data [6, 7]. From Fig. 4, we see that the

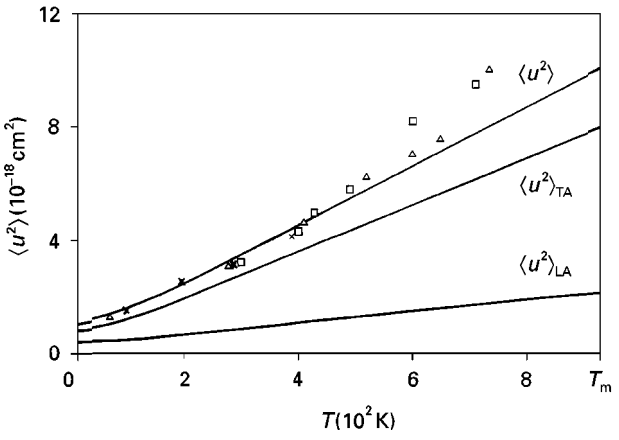

Figure 1 The calculated mean-square displacements, $\langle u^2 \rangle$, $\langle u^2 \rangle_{TA}$ and $\langle u^2 \rangle_{LA}$ versus temperature for matrix Al. (△), observed data [3]; (□), observed data [4]; (×), observed data [5].

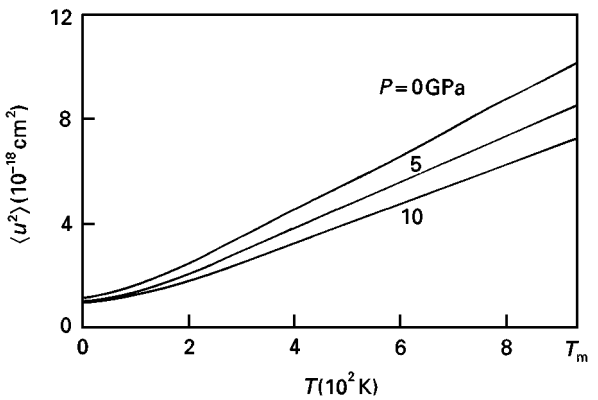

Figure 2 The calculated mean-square displacement, $\langle u^2 \rangle$, under pressure versus temperature for matrix Al.

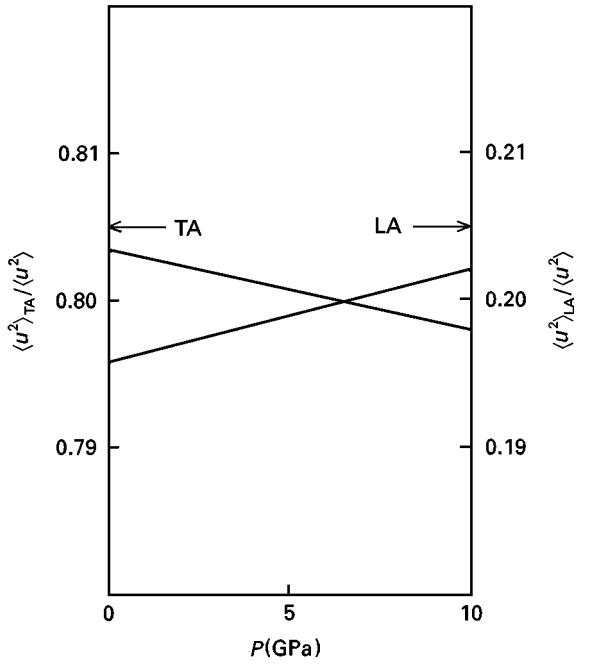

Figure 3 The relative ratios, $\langle u^2\rangle_{TA}/\langle u^2\rangle$ and $\langle u^2\rangle_{TA}/\langle u^2\rangle$, versus pressure at the melting point, T_m, under atmospheric pressure for matrix Al.

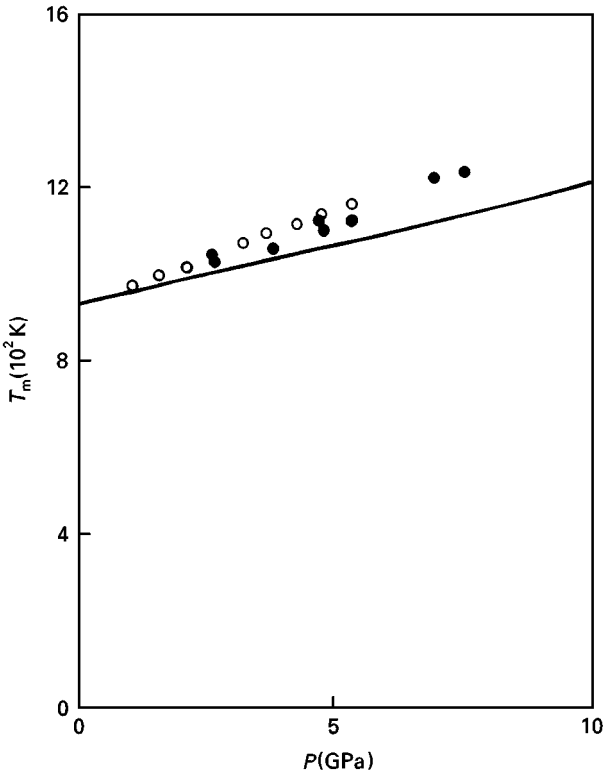

Figure 4 The calculated melting point, T_m, versus pressure for matrix Al. (○), observed data [6]; (●), observed data [7].

melting temperature of matrix Al increases under increasing pressure and this tendency obtained is consistent with the observed data [6, 7].

3. Solidus curve under pressure of the Al–Si and Al–Ge systems

Formulations for matrix Al in Section 2 are extended to those for the Al–Si and Al–Ge alloy systems as

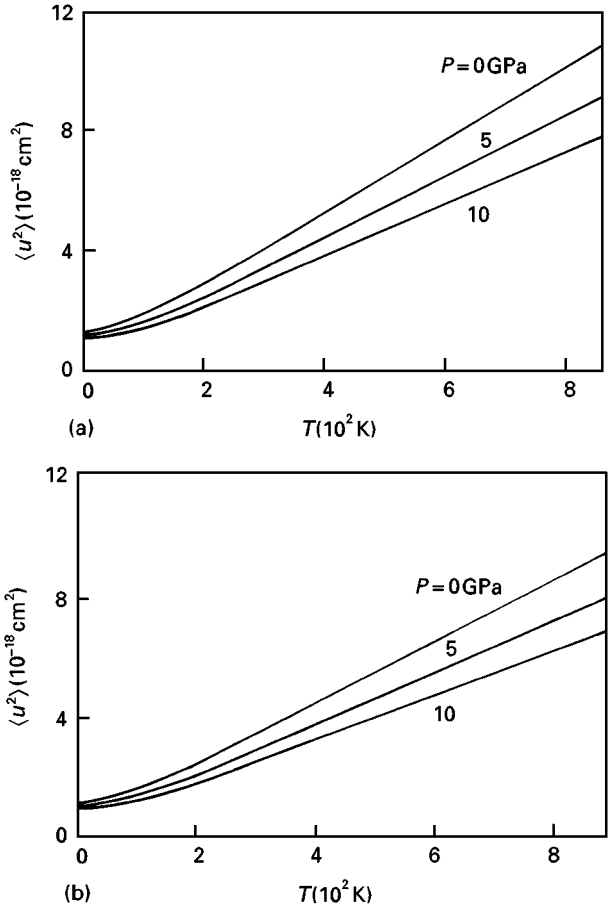

Figure 5 The calculated mean-square displacement, $\langle u^2\rangle$, under pressure versus temperature for (a) $Al_{0.85}Si_{0.15}$ and (b) $Al_{0.85}Ge_{0.15}$ alloys.

follows. Considering the band and local mode frequencies, $\nu_i^j(\boldsymbol{q}, x)$ [13] in the $Al_{1-x}Si_x$ and $Al_{1-x}Ge_x$ solid solutions, the mean-square displacement, $\langle u^2\rangle_x$, for these alloy systems is given by

$$\langle u^2\rangle_x = (1-x)\frac{h}{NM^{Al}}U^{Al}(x) + x\frac{h}{NM^{Si\text{ or }Ge}}U^{Si\text{ or }Ge}(x) \quad (7)$$

and

$$U^j(x) = \sum_{i,q}\frac{1}{\nu_i^j(\boldsymbol{q}, x)}\left(\frac{1}{\exp[h\nu_i^j(\boldsymbol{q}, x)/kT\,]-1}+\frac{1}{2}\right) \quad (8)$$

where j = Al, Si or Ge. We show the temperature dependence of the mean-square displacement, $\langle u^2\rangle$, for the $Al_{0.85}Si_{0.15}$ and $Al_{0.85}Ge_{0.15}$ solid solutions obtained using Equations 7 and 8 in Fig. 5a and b, respectively. From Fig. 5, we see that the pressure effect on the mean-square displacement for these alloy systems is similar to that for matrix Al in Fig. 2.

We can estimate the Debye temperatures Θ_D^{ht} and Θ_D^{lt} at high and low temperatures in Equations 2 and 3. We show the obtained concentration x dependence of the Debye temperature Θ_D^{ht} at the representative temperatures, which are taken to be 850 K and 680 K for the $Al_{1-x}Si_x$ and $Al_{1-x}Ge_x$ solid solutions, and Θ_D^{lt} at the absolute zero in Figs 6 and 7, respectively. Our

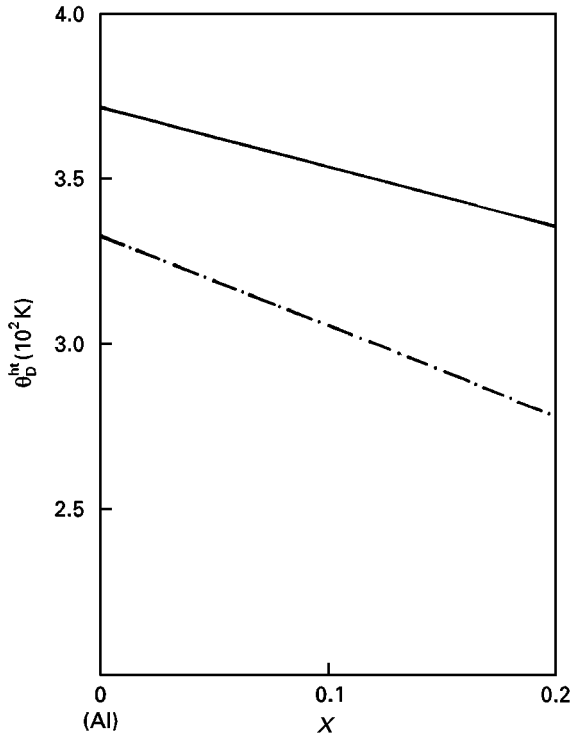

Figure 6 The calculated Debye temperature, Θ_D^{ht}, at 850 and 680 K versus atomic fraction for $Al_{1-x}Si_x$ (—) and $Al_{1-x}Ge_x$ (—·—).

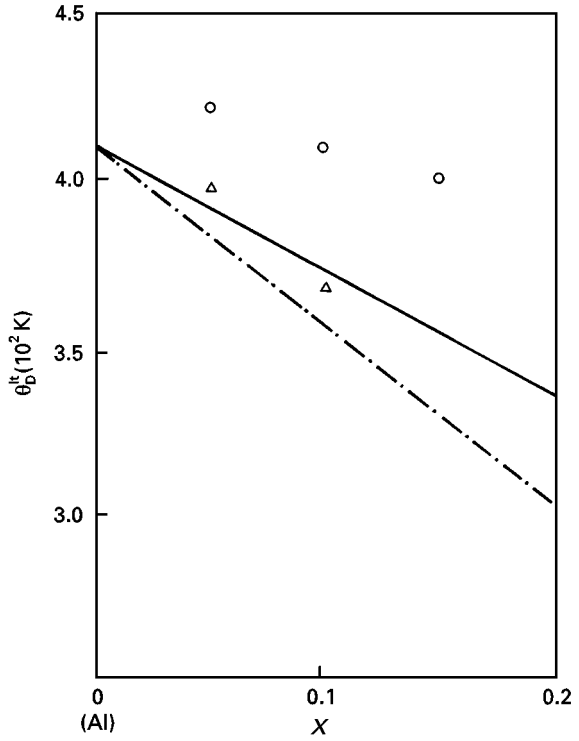

Figure 7 The calculated Debye temperature, Θ_D^{lt}, at absolute zero versus atomic fraction for $Al_{1-x}Si_x$ (—) and $Al_{1-x}Ge_x$ (—·—). (□), observed data [17, 18] for matrix Al; (○), observed data [17, 18] for $Al_{1-x}Si_x$; (△), observed data [17, 18] for $Al_{1-x}Ge_x$ alloy.

obtained Debye temperature Θ_D^{ht} and Θ_D^{lt} in Figs 6 and 7 have a calculated accuracy $|\Delta\Theta_D| \leqslant 4$ K due to other screening functions [11]. Our obtained data Θ_D^{lt} for matrix Al are in good agreement with the observed data

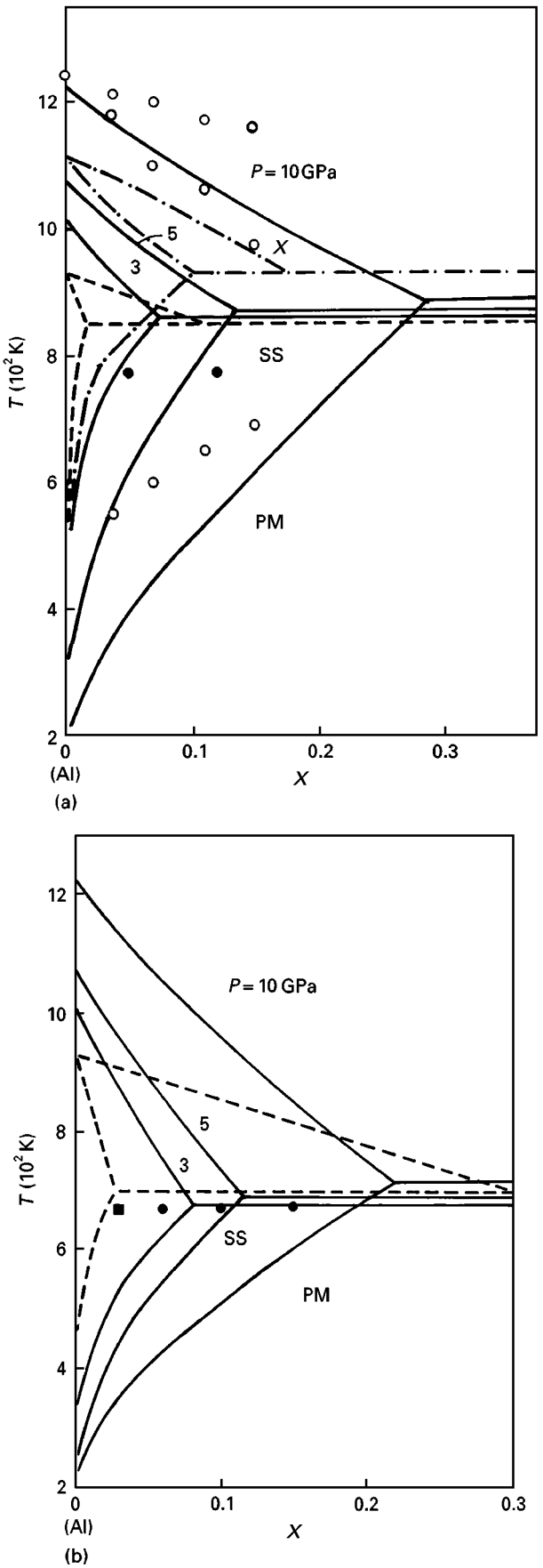

Figure 8 The resultant solidus curves under pressure for (a) $Al_{1-x}Si_x$ and (b) $Al_{1-x}Ge_x$ systems. The phase boundaries between solid solution (SS) and phase mixture (PM) under pressure are our previous data [11]. (– – –) $P = 0$ GPa [8]; (–·–), $P = 2.8$ GPa [9]; (○), $P = 5.4$ GPa [9]; (■), solid solution with the f.c.c. phase [10] obtained experimentally at $P = 4.5$ GPa; (●), solid solution with the f.c.c. phase [10] obtained experimentally at $P = 7.0$ GPa; (×), solid solution with the f.c.c. phase [10] obtained experimentally at $P = 9.0$ GPa.

[17] from elastic waves. The relative change in the Debye temperature $\Delta\Theta_D(x) = \Theta_D(x) - \Theta_D(x = 0)$ from that for matrix Al have a reduced accuracy $|\Delta\Theta_D(x)| \leqslant 1.5$ K due to other screening functions [11]. From Figs 6 and 7, we see that the Debye temperature decreases with increasing solubility of Si or Ge at high temperatures and decreases greatly at low temperatures.

Using the concentration-dependent mean-square displacement, $\langle u^2 \rangle_x$, in Equations 7 and 8 for the $Al_{1-x}Si_x$ and $Al_{1-x}Ge_x$ alloy systems, we define Lindeman's criterion for melting, $x_m(x)$, of these alloys as the ratio of twice the root-mean-square displacement, $\langle u^2 \rangle_x^{1/2}$, at the corresponding temperature, $T_m(x)$, on the solidus curve [8] under atmospheric pressure to the nearest-neighbour distance $R_1(x) (= 2^{1/2}a(x)/2)$ given by

$$x_m(x) = \frac{2\langle u^2 \rangle_x^{1/2}}{R_1(x)} \tag{9}$$

where $a(x)$ is the equilibrium lattice constant [11] for these systems. We obtain the critical fraction, $x_m(x)$, in Equation 9 to be 0.2214 in the solubility limit [8] under atmospheric pressure with $x = 0.016$ at $T = 850$ K for the $Al_{1-x}Si_x$ alloy and 0.2212 with $x = 0.028$ at $T = 697$ K for $Al_{1-x}Ge_x$. The slope $\Delta x_m/(x_m \Delta x)$ is -0.0564 for the $Al_{1-x}Si_x$ and -0.0644 for the $Al_{1-x}Ge_x$ system. Because the concentration dependence of x_m is small and remains within Lindeman's melting law [15, 16], we adopt the extrapolated dependence of this slope, $\Delta x_m/(x_m \Delta x)$, outside the solubility limit under atmospheric pressure.

Considering the pressure dependence of the mean-square displacement, $\langle u^2 \rangle_x$, and the nearest-neighbour distance, $R_1(x)$, for $Al_{1-x}Si_x$ and $Al_{1-x}Ge_x$ solid solutions at a constant criterion for melting, $x_m(x)$, we can estimate the pressure effect on the solidus curve for these alloys by satisfying the following relations

$$x_m(x) = \frac{2\langle u^2 \rangle_{x, T_m(x,P)}^{1/2}}{R_1(x, P)} \tag{10}$$

and

$$R_1(x, P) = \left(\frac{\Omega(x, P)}{\Omega_0(x)}\right)^{1/3} R_1(x, \Omega_0) \tag{11}$$

where the conversion from the pressure, $P(x)$, to the compressed volume, $\Omega(x)$, is done using the pressure–volume relations [11]. We show the obtained solidus curve under pressure for the $Al_{1-x}Si_x$ and $Al_{1-x}Ge_x$ alloy systems in Fig. 8a and b, respectively. From Fig. 8, we see that the solid solution in Al–Si and Al–Ge system, extended under pressure, is consistent with the observed tendency [9, 10]. Our resultant solidus curves in Fig. 8 have a calculated accuracy corresponding to $|\Delta x| \leqslant 0.01$ and $|\Delta T| \leqslant 5$ K. We present the phase diagrams under pressure for Al–Si and Al–Ge systems from first principles based on the microscopic electronic theory, and we hope that there will be further experimental research in this field. The numerical calculations were carried out with the ACOS3900 operating system at the Computer Center of Tohoku University.

References

1. F. LINDEMAN, *Z. Phys.* **11** (1910) 609.
2. N. KAWAI and Y. INOKUTI, *Jpn. J. Appl. Phys.* **7** (1968) 989.
3. E. A. OWEN and R. W. WILLIAMS, *Proc. R. Soc. A* **188** (1947) 509.
4. D. R. CHIPMAN, *J. Appl. Phys.* **31** (1960) 2012.
5. P. A. FLINN and C. M. McMANUS, *Phys. Rev.* **132** (1963) 2458.
6. A. JAYARAMAN, W. KLEMENT, R. C. NEWTON and G. C. KENNEDY, *J. Phys. Chem. Solids* **24** (1963) 7.
7. J. F. CANNON, *J. Phys. Chem. Ref. Data* **3** (1974) 781.
8. M. HANSEN, "Constitution of binary alloys" (McGraw-Hill, New York, 1958).
9. H. MII, M. SENOO and I. FUJISHIRO, *Jpn. J. Appl. Phys.* **15** (1976) 777.
10. V. F. DEGTYAREVA, G. V. CHIPENKO, I. T. BELASH, O. I. BARKALOV and E. G. PONYATOVSKII, *Phys. Status Solidi* (*a*) **89** (1985) K127.
11. T. SOMA, Y. FUNAYAMA and H.-M. KAGAYA, *J. Mater. Sci.* **25** (1990) 3917.
12. T. SOMA, S. TAKASHIMA and H.-M. KAGAYA, *ibid.* **27** (1992) 1184.
13. T. SOMA, I. KITABATAKE and H.-M. KAGAYA, *ibid.* **29** (1994) 640.
14. J. M. ZIMAN, "Principle of the theory of solids" (Cambridge University Press, Cambridge, 2nd Edn, 1976) Ch. 2.
15. A. K. SINGH and P. K. SHARMA, *Can. J. Phys.* **46** (1968) 1677.
16. J. S. REID and T. SMITH, *J. Phys. Chem. Solids* **31** (1970) 2689.
17. C. KITTEL, "Introduction to solid state physics" (Wiley, New York, 6th Edn, 1986) Ch. 5.
18. A. MATSUMURO, K. MURATA, K. SAKAI and M. SENOO, *J. Mater. Sci.* **28** (1993) 5836.

Received 3 April 1997
and accepted 5 February 1998